

Thermal and Transport Behavior of Single Crystalline R_2CoGa_8 ($R = Gd, Tb, Dy, Ho, Er, Tm, Lu$ and Y) Compounds

Devang A. Joshi, A. K. Nigam, S. K. Dhar and A. Thamizhavel

*Department of Condensed Matter Physics and Material Sciences,
Tata Institute of Fundamental Research, Homi Bhabha Road, Colaba, Mumbai 400 005, India.*

The anisotropy in electrical transport and thermal behavior of single crystalline R_2CoGa_8 series of compounds is presented. These compounds crystallize in a tetragonal structure with space group $P4/mmm$. The nonmagnetic counterparts of the series namely Y_2CoGa_8 and Lu_2CoGa_8 show a behavior consistent with the low density of states at the Fermi level. In Y_2CoGa_8 , a possibility of charge density wave transition is observed at ≈ 30 K. Gd_2CoGa_8 and Er_2CoGa_8 show a presence of short range correlation above the magnetic ordering temperature of the compound. In case of Gd_2CoGa_8 , the magnetoresistance exhibits a significant anisotropy for current parallel to $[100]$ and $[001]$ directions. Compounds with other magnetic rare earths ($R = Tb, Dy, Ho$ and Tm) show the normal expected magnetic behavior whereas Dy_2CoGa_8 exhibits the possibility of charge density wave (CDW) transition at approximately same temperature as that of Y_2CoGa_8 . The thermal property of these compounds is analysed on the basis of crystalline electric field (CEF) calculations.

PACS numbers: 71.20.Eh, 71.70.Ch, 72.15.Eb, 73.43.Qt, 74.25.Ha and 75.50.Ee
Keywords: Antiferromagnetism, Schottky, CEF, CDW, Magnetoresistance

I. INTRODUCTION

Recently we reported the magnetic properties of single crystalline R_2CoGa_8 series of compounds, inferred from the thermal and field dependence of magnetization (**author?**) [1]. These compounds form only with the heavy rare earths ($R = Gd$ to Lu), in contrast to the iso-structural indides R_2CoIn_8 (**author?**) [2] where the phase forms for all the rare earths except for La, Yb and Lu . Y_2CoGa_8 and Lu_2CoGa_8 show diamagnetic behavior pointing out a relatively low density of states at the Fermi level. R_2CoGa_8 with magnetic rare earths order antiferromagnetically at low temperatures with the highest Néel temperature $T_N = 28$ K in Tb_2CoGa_8 . The magnetic ordering temperatures are less compared to their corresponding indides. The easy axis of magnetization for Tb_2CoGa_8 , Dy_2CoGa_8 and Ho_2CoGa_8 was found to be along the $[001]$ direction whereas for Er_2CoGa_8 and Tm_2CoGa_8 the easy axis changes to the basal plane namely (100) . Gd_2CoGa_8 having the S -state ion Gd^{3+} was found to show isotropic magnetic behavior. A point charge model calculation of the crystal electric field (CEF) effects gave a qualitative explanation of the magnetocrystalline anisotropy in this series of compounds and the appreciable deviation of the ordering temperatures in Tb_2CoGa_8 and Dy_2CoGa_8 from that expected on the basis of de-Gennes scaling. The aim of the present paper is to investigate in detail the heat capacity and electrical transport properties of R_2CoGa_8 compounds to get more information about the crystal electric field effects, Schottky contribution to the heat capacity, entropy associated with the magnetic ordering,

etc. The magnetoresistivity was also studied keeping in mind the anomalously high magnetoresistance ($\sim 2700\%$ at 2 K) of Tb_2CoIn_8 (**author?**) [2].

II. EXPERIMENTAL

Single crystals of R_2CoGa_8 compounds were grown using Ga flux as described elsewhere (**author?**) [1]. An energy dispersive X-ray analysis (EDAX) was performed on all the obtained single crystals to estimate the actual crystal composition. The EDAX results confirmed the crystals to be of the stoichiometric composition 2:1:8. To check for the phase purity, powder x-ray diffraction pattern of all the compounds were recorded by powdering a few small pieces of single crystal followed by the Rietveld analysis of the obtained pattern. For the anisotropic transport measurements, the single crystals were oriented along the principle directions viz., $[100]$ and $[001]$ by Laue back reflection method. The crystals were cut to the required size for resistivity and heat capacity measurements using a spark erosion wire cutting machine. The heat capacity, resistivity and magnetoresistance measurements were performed using physical property measurement system (PPMS - Quantum Design). The AC susceptibility of Gd_2CoGa_8 and Tb_2CoGa_8 was also measured in MPMS - Quantum Design.

III. RESULTS AND DISCUSSION

A. Y_2CoGa_8 and Lu_2CoGa_8

We first present the data on Y_2CoGa_8 and Lu_2CoGa_8 , which are the nonmagnetic analogs of the R_2CoGa_8 compounds, Co being non-magnetic in this family of compounds. As mentioned above Y_2CoGa_8 and Lu_2CoGa_8 show diamagnetic behavior, in contrast to the indide Y_2CoIn_8 (**author?**) [2], which is Pauli-paramagnetic. The diamagnetic contribution arises from the filled electronic shells, which dominate a modest Pauli-paramagnetic contribution arising from a low density of the conduction electron states at the Fermi level $N(E_F)$. The evidence for low $N(E_F)$ comes from the low temperature (1.8 to 10 K) heat capacity data which furnish γ values of 2 and 4 mJ/mole K^2 for Y_2CoGa_8 and Lu_2CoGa_8 respectively (Fig. 1a inset). These values are low in comparison to the corresponding indide Y_2CoIn_8 (12 mJ/mole- K^2). An estimate of the density of states at the Fermi level is obtained using the free electron relation

$$\gamma = \frac{2}{3} \pi^2 k_B^2 N(E_F) \quad (1)$$

where k_B is the Boltzmann constant. Substituting the value of $\gamma = 2$ mJ/mole- K^2 , the density of states in Y_2CoGa_8 , for example, is found to be 1.6×10^{35} erg $^{-1}$ mole $^{-1}$ or 5.8 Ry $^{-1}$ atom $^{-1}$. This value, for ex-

ample, is comparable to that obtained in the diamagnetic compound YPd_3 (**author?**) [3] from band structure calculations. In the free electron approximation γ and the Pauli susceptibility χ_0 are related by the relation: $\gamma(mJ/mole K^2) = 1.3715 \times 10^{-5} \chi_0(emu/mole)$. For Y_2CoGa_8 and Lu_2CoGa_8 the gamma values furnish χ_0 less than 10^{-4} emu/mol. On the other hand using the relation for diamagnetic contribution $\chi_{Dia} \approx -10^{-6} Z$, where Z is the atomic number, we infer χ_{Dia} values of -3.5×10^{-4} and -4.2×10^{-4} emu/mole for Y and Lu compounds, respectively, which in absolute magnitude are higher than χ_0 . Replacing indium fully by gallium results in the appearance of diamagnetism. Since the valency of both In and Ga is same (both of them have one extra p electron), it is possible that shrinking of the unit cell in gallides results in shifting of the Fermi level to a region of low density of states.

From the slope of C/T vs T^2 plots (inset Fig. 1a) we infer the lattice heat capacity coefficient β as 0.501 and 0.782 mJ/mole K^4 in Y_2CoGa_8 and Lu_2CoGa_8 , respectively. Using the relation of the Debye model $\Theta_D^3 = 1943600/\beta$, where β is in the units of mJ/g atom K^4 and Θ_D is the Debye temperature, we obtain $\Theta_D = 349$ and 301 K in Y_2CoGa_8 and Lu_2CoGa_8 , respectively. Based on the Debye approximation(**author?**) [6],

$$\frac{\Theta_D(Y_2CoGa_8)}{\Theta_D(Lu_2CoGa_8)} = \sqrt{\frac{MW(Lu_2CoGa_8)}{MW(Y_2CoGa_8)}} \quad (2)$$

the ratio of the Debye temperatures is 1.16 in fair agreement with the r.h.s value of 1.4.

The main panel of Fig. 1 shows the heat capacity of Lu_2CoGa_8 and Y_2CoGa_8 from 1.8 to 160 K. The heat capacity curve for Y_2CoGa_8 was fitted to the equation

$$C_{Tot} = \gamma T + C_{Ph} \quad (3)$$

where the two terms represents the electronic and phononic contributions, respectively. C_{Ph} can be written in terms of Debye integral as

$$C_{Ph} = 9NR \left(\frac{T}{\Theta_D} \right)^3 \int_0^{\Theta_D/T} \frac{x^4 e^x dx}{(e^x - 1)^2} \quad (4)$$

where $x = \Theta_D/T$, N is the number of atoms in the formula unit and Θ_D is the Debye temperature. Here γ was fixed to the values derived above and $N = 11$. The best fit shown by solid line in Fig. 1 is obtained with $\Theta_D = 291$ K. This value of Θ_D is lower than that derived above, which may be due to the variation of Θ_D with temperature. Around ≈ 30 K the fit for Y_2CoGa_8 is relatively poor for which a possible reason is mentioned below.

Fig. 1(b) shows the resistivity curves for the Y_2CoGa_8 compound with current (J) parallel to the crystallographic directions [100] and [001], respectively. Along

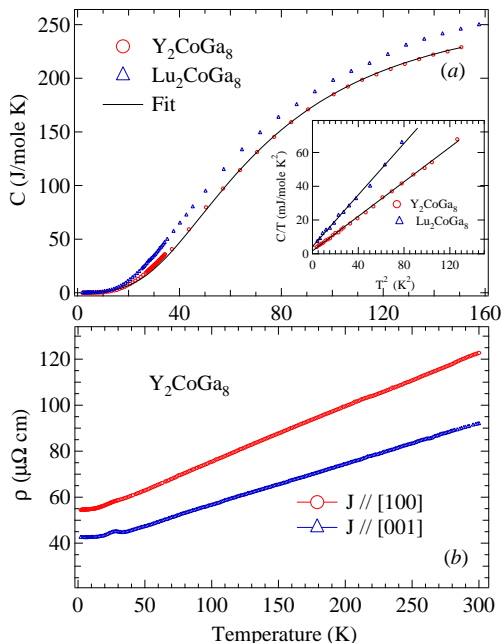


Figure 1: (a) Heat capacity curve of Lu_2CoGa_8 and Y_2CoGa_8 with a fit described in text. The inset shows the C/T vs T^2 plot. (b) Resistivity of Y_2CoGa_8 with the current parallel to [100] and [001] directions.

both the directions the temperature dependent resistivity demonstrates a metallic behavior, the resistivity decreases linearly at high temperatures followed by a nearly temperature independent behavior below 15 K. The observed behavior is in tune with the phonon-induced scattering of the charge carriers expected in a non-magnetic compound. There occurs a hump between 20 and 35 K which is more prominent along [001] direction. A similar hump was also found in polycrystalline Y_2CoIn_8 (author?) [2]. Such a hump in the resistivity of a nonmagnetic compound is rarely seen and may arise due to a charge density wave induced formation of an anisotropic energy gap in the Fermi surface. Similar behavior is also seen in case of 2H-NbSe_2 , Nb_3Te_4 , 2H-TaSe_2 , NbSe_3 , ZrTe_3 , LaAgSb_2 , etc (author?) [4, 5, 7, 8, 9]. The absence of hysteresis in resistivity indicates a second order nature of the proposed charge density wave transition. The prominent effect along the [001] may be due to a larger gap along this direction. The deviation of the fit based on the Debye formula to the heat capacity around 30 K (Fig. 1(a)) may also be due to the same effect. The resistivity along [001] direction is found to be lower compared to the in-plane [100] resistivity. The similar anisotropic behavior in the resistivity was found for all the compounds described below and may arise due to the inherent structural anisotropy of the compound. The residual resistivity along [100] and [001] directions is $42 \mu\Omega \text{ cm}$ and $54 \mu\Omega \text{ cm}$ respectively. Overall, the resistivity values are higher compared to corresponding polycrystalline indide Y_2CoIn_8 (author?) [2]. It may be due to the low density of states at the Fermi level in Y_2CoGa_8 . A similar observation on Lu_2CoGa_8 would have strengthened our conjecture but single crystals of Lu_2CoGa_8 were too small for resistivity measurements.

B. Gd_2CoGa_8

The results on Gd_2CoGa_8 are presented next as Gd is an S -state ion and the CEF effects are negligible in the first order approximation. Fig. 2(a) shows the temperature dependence of resistivity for Gd_2CoGa_8 with current parallel to [100] and [001] directions, respectively. The inset shows the expanded low temperature part below 37 K. The resistivity shows a metallic behavior with temperature down to 35 K. Similar to Y_2CoGa_8 the resistivity with current along [100] direction is higher than along [001]. Below 35 K the resistivity with current parallel to [100] levels off followed by a minor kink at $T_N = 20$ K and then it drops almost linearly down to 2 K. The upward kink at T_N can be attributed to a small gap introduced in the Fermi surface due to the magnetic super-zone effect (author?) [11]. The resistivity with current along [001] direction shows an apparently anomalous behavior. It increases below 35 K in the paramagnetic region well above the ordering temperature followed by a sharp increase at T_N and then decreases at low temperatures.

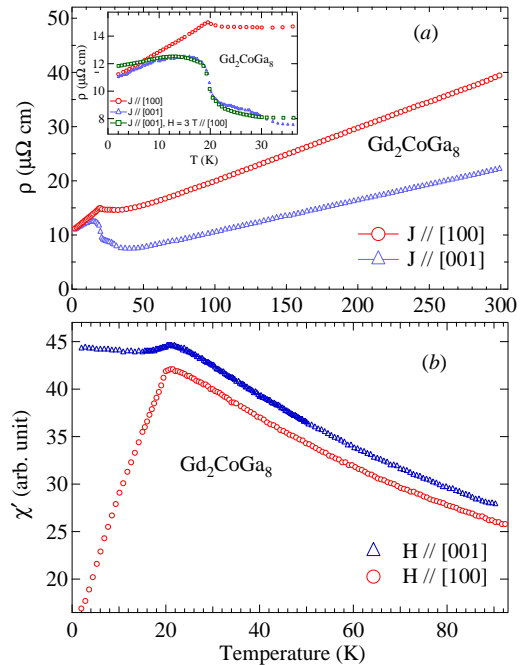


Figure 2: (a) Resistivity of Gd_2CoGa_8 with current parallel to [100] and [001] direction. The inset shows the expanded low temperature part. (b) AC susceptibility for the same with AC field parallel to [100] and [001] directions.

The decrease is not as sharp as expected from the loss in spin disorder resistivity but tends to fall slowly. The sharp rise at T_N is due to the dominant super-zone gap effect along [001]. The rise in resistivity in the paramagnetic state as the temperature approaches T_N , is most likely due to the short range antiferromagnetic correlations (author?) [12, 13]. It has been shown theoretically that the temperature derivative of resistivity has a negative divergence as T_N is approached from the paramagnetic regime due to the large angle scattering and the divergence in the spin-spin correlation function at Néel temperature (author?) [12] and in reality it is the life time of the anomalous fluctuation is masked by the energy transfer from the conduction electrons resulting in the increase in the resistivity of the compound. Some antiferromagnetic compounds are known to show similar behavior; for example: Tb (author?) [14], $(\text{RPd}_3)_8\text{Al}$ ($R = \text{Tb}$ and Gd) (author?) [15], UNiAl (author?) [16]. When a magnetic field of 30 kOe is applied along the [100] direction, the upturn in the resistivity in the paramagnetic state between ≈ 30 K and T_N is partially suppressed as shown in the inset of Fig. 2(a). The suppression of the upturn in resistivity with field supports the short range antiferromagnetic correlation in the compound along the [001] axis. Above 30 K, the crossover in the $H = 0$ and 30 kOe plots is likely due to the positive cyclotron contribution of the charge carriers to magneto-resistance.

The anisotropic behavior of resistivity in the neighbor-

hood of T_N in contrast to the corresponding isotropic behavior of DC magnetization (5 kOe) (author?) [1] motivated us to investigate Gd_2CoGa_8 with AC susceptibility. The data are shown in Fig.2(b), with the AC field applied along the two crystallographic directions. χ' along [100] increases in the paramagnetic state followed by a peak at T_N and then decreases as expected for a simple antiferromagnet. On the other hand, along [001] direction χ' does not decrease below T_N and shows a slight upturn at low temperatures, indicating the presence of complicated magnetic structure with anisotropy. The interaction of the charge carriers with anisotropic magnetic configuration is responsible for the observed behavior of resistivity around T_N .

The transverse magnetoresistance (MR), defined as $MR = [R(H)-R(0)]/R(0)$, of the compound at 2 K with current applied along the two principal crystallographic directions shows significant anisotropy (Fig. 3(a)). With current along [100] the MR increases almost linearly with field up to approximately 12 % at 90 kOe, whereas along [001] direction it varies more strongly increasing nonlinearly up to 57 % at 90 kOe. The contribution to the total MR due to spin-orbit coupling will be negligible for Gd^{3+} ions. The cyclotron contribution will also not give rise to such a large MR. Field induced metamagnetic transitions can give rise to a large MR, but Gd_2CoGa_8 does not show any metamagnetic behavior at 2 K and further the magnetic isotherms at 2 K along both the directions nearly coincide with each other (author?) [1] thereby pointing out that the magnetoresistivity behavior in Gd_2CoGa_8 is primarily influenced by other factors. Further with both current and field constrained to ab plane ($J // [100]$ and $H // [010]$) but transverse to each other, the magnetoresistance increases to 5 % at 90 kOe. Hence the direction of the field does not play a major role for anomalously high magnetoresistance with current parallel to [001] and only the direction of the current matters. We suggest that the anisotropy in MR arises due to the anisotropy of the Fermi surface. The heat capacity behavior of Gd_2CoGa_8 is shown in Fig. 3(b). It undergoes a lambda type second order magnetic transition at $T_N = 20$ K consistent with the magnetic susceptibility and resistivity data. The magnetic contribution to the heat capacity was isolated using the data for Lu_2CoGa_8 , assuming it as a measure of phonon contribution, taking into account the mass difference between Gd and Lu. The magnetic entropy calculated as a function of temperature is shown in the inset of Fig. 3(b). The entropy at T_N is 13 J/mole K and it attains the theoretical value of $R \ln 8$ (17.3 J/mole K) at about 60 K. It nearly saturates above 60 K. This indicates the presence of short range antiferromagnetic correlations above T_N and provides further support to our explanation of the upturn in the resistivity in the paramagnetic state as mentioned above.

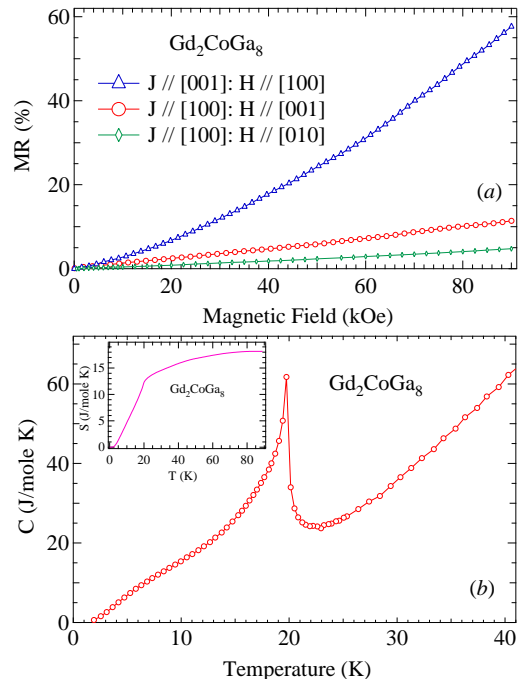


Figure 3: (a) Magnetoresistance of Gd_2CoGa_8 with current parallel to [100] and [001] directions. (b) Heat capacity of Gd_2CoGa_8 with inset showing the calculated magnetic entropy.

C. Tb_2CoGa_8 , Dy_2CoGa_8 and Ho_2CoGa_8

We now describe our results for compounds in which CEF effects are operative. In ref.1 (author?) [1], it was found that for compounds with Tb, Dy and Ho, the easy axis of magnetization is along [001]. The resistivity of Tb_2CoGa_8 with current parallel to [100] and [001] directions, respectively, is shown in Fig. 4(a). The resistivity along both the directions initially decreases linearly with temperature down to ≈ 130 K followed by a relatively faster drop at lower temperatures, which we attribute to the CEF effect. The thermally induced variation of the fractional Boltzmann occupation of the CEF levels changes the otherwise constant spin disorder resistivity. Overall, the decreases in the resistivity between 1.8 and 300 K is more prominent for $J // [100]$ ($\approx 200 \mu\Omega$ cm) than for $J // [001]$ ($\approx 30 \mu\Omega$ cm), indicating a significant anisotropy in the transport property of the compound. A change in the slope at T_N for $J // [001]$ (see, inset) occurs due to the loss of spin disorder resistivity. There is no discernible anomaly at T_N for $J // [100]$ but a change in slope exists below 15 K. To investigate a possible origin of this feature, the AC susceptibility was measured with AC field along [100] and [001] directions as shown in Fig. 4(b). It decreases monotonically below T_N along [001] but along the [100] direction it increases below 15 K followed by a peak at ≈ 6 K. The change in the slope of resistivity at 15 K thus appear to be correlated to the

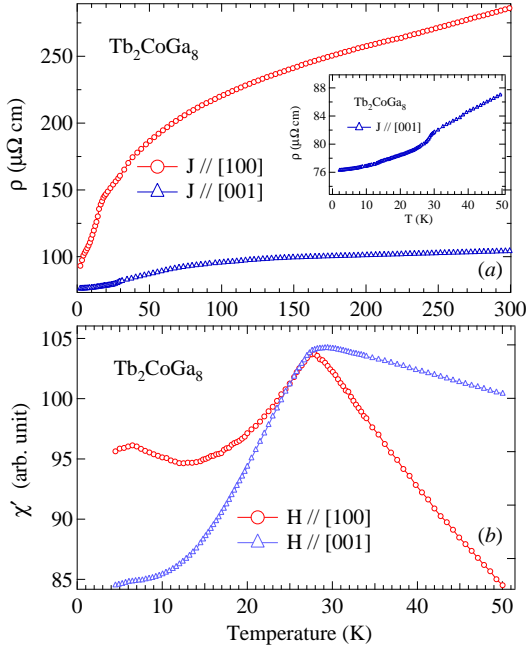


Figure 4: (a) Resistivity of Tb₂CoGa₈ with current parallel to [100] and [001] directions, respectively. (a) AC susceptibility of Tb₂CoGa₈ with AC field parallel to [100] and [001] directions, respectively.

behavior of the AC susceptibility below 15 K. It is possible that because of some complicated magnetic structure there is a component along the *ab*-plane whose variation with temperature affects the variation of resistivity. The magnetoresistance of the compound with current parallel to [100] and [001] directions, respectively, is shown in Fig. 5(a). The positive magnetoresistance along both the crystallographic directions is consistent with the antiferromagnetic behavior of the compound. Magnetoresistance at 2 K with $H // [100]$ and $J // [001]$ increases almost linearly by 17 % with applied field increased to 90 kOe. On the other hand the magnetoresistance shows a complex behavior for $H // [001]$. At 2 K for $J // [100]$, MR initially increases linearly with field. There is a rapid increase in a narrow interval near $H \sim 35$ kOe followed by a distinct change in the variation near 82 kOe. The magnetoresistance at 90 kOe is ≈ 77 %, which though appreciable is far less than that of the corresponding indide Tb₂CoIn₈ (~ 2700 % at 2 K). The anomalies at 42 and 82 kOe are consistent with the metamagnetic transitions observed in the magnetic isotherm of the compound at 2 K along the easy axis as reported in ref.1 (author?) [1]. At 5 K, the magnetoresistance decreases but qualitatively the behavior is similar to that at 2 K. Increasing the temperature to 10 K, the first anomaly in MR is slightly shifted up in field whereas above 80 kOe the magnetoresistance decreases with field. The latter is due to the reduction in the scattering of the conduction electrons by the ferromagnetically aligned Tb³⁺ ions at high

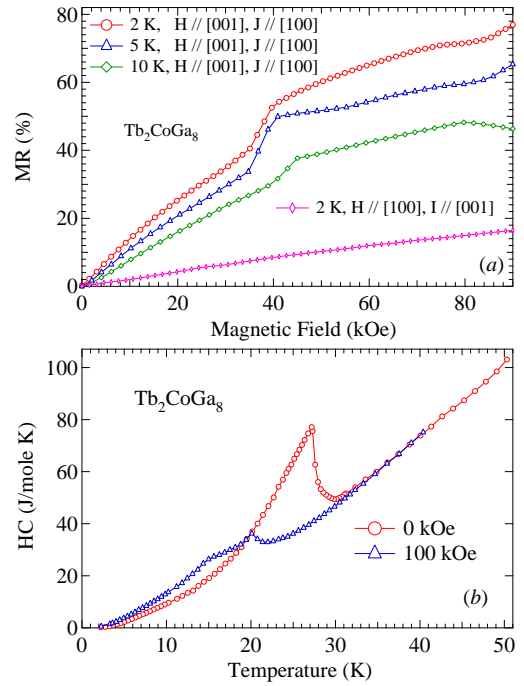


Figure 5: (a) Magnetoresistance for Tb₂CoGa₈ with current and field in the indicated direction. (b) Heat Capacity for the same with and without field.

fields where the compound enters the field induced ferromagnetic state. Here the field-induced polarized state is achieved by the combined action of field and temperature (~ 80 kOe and 10 K, respectively). Higher fields are required to induce the ferromagnetic state at lower temperatures. The heat capacity of the Tb₂CoGa₈ (Fig. 5(b)) in zero field is dominated by a lambda type anomaly at the Néel temperature ($T_N = 27.5$ K). In an applied field of 100 kOe the anomaly disappears; a broad hump and a kink appear at lower temperatures, reflecting an overall weakening of the antiferromagnetic configuration in applied fields and field induced metamagnetic transition in the compound.

The *4f* contribution to the heat capacity, C_{4f} , determined using the same procedure as mentioned for Gd₂CoGa₈, and the entropy S_{4f} is shown in Fig. (6). In addition we have also plotted the Schottky specific heat C_{Sch} and the corresponding entropy S_{Sch} calculated from the following expressions

$$C_{Sch} = \frac{\partial}{\partial T} \left[\frac{1}{Z} \sum_n E_n \exp\left(-\frac{E_n}{k_B T}\right) \right] \quad (5)$$

$$S_{4f, Sch} = \int_0^T \frac{C_{4f, Sch}}{T} dT \quad (6)$$

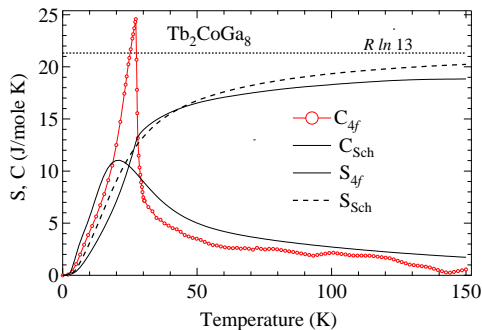


Figure 6: The $4f$ contribution C_{4f} to the heat capacity of Tb_2CoGa_8 with Schottky contribution C_{Sch} estimated from CEF split energy levels. The corresponding entropies estimated from $4f$ contribution and CEF split levels are also shown.

where, Z is the partition function, E_n are the CEF split energy levels derived from the CEF fitting of the inverse magnetic susceptibility in ref.1 (author?) [1]. It is evident from the figure that there is a reasonably good agreement between C_{4f} and C_{Sch} in the paramagnetic regime. This supports the validity of the CEF level scheme for Tb_2CoGa_8 as derived from the magnetization data. The entropy obtained from the magnetic contribution to the heat capacity is 18.9 J/mole K at 150 K. The theoretically expected value of $R \ln(2J + 1)$ (21.32 J/mole K) will be achieved at higher temperatures when all the CEF levels are thermally populated.

The temperature dependence of electrical resistivity from 1.8 to 300 K for Dy_2CoGa_8 is shown in Fig. 7(a). The high temperature part of the electrical resistivity of Dy_2CoGa_8 is qualitatively similar to that of Tb_2CoGa_8 along the two crystallographic directions, whereas the low temperature resistivity shows a different behavior. The resistivity for $J // [100]$ decreases monotonically below 50 K and does not show any anomalies and becomes nearly temperature independent below 20 K. Along [001] the resistivity shows peaks at ≈ 29 and 6 K, the former in the paramagnetic state and the latter below T_N . The increase in the resistivity below T_N (17 K) is due to the super-zone gap effects, and it is also consistent with the magnetization results which show that the moments order along the [001] direction. In order to look for possible origin of the paramagnetic peak at 29 K, we measured the AC susceptibility with field along [001] direction (not shown). However, no anomaly was found in AC susceptibility; neither do we observe any anomaly at 29 K in the heat capacity (may be overridden by the magnetic contribution) (Fig. 8(a)). The sharp drop in resistivity below ≈ 29 K (Fig. 7(a) inset) with decreasing temperature rules out the possibility of spin fluctuation. The ≈ 29 K peak in Dy_2CoGa_8 exists nearly at the same temperature as in Y_2CoGa_8 . Hence it may also be due to a charge density wave induced gap in the Fermi surface as speculated

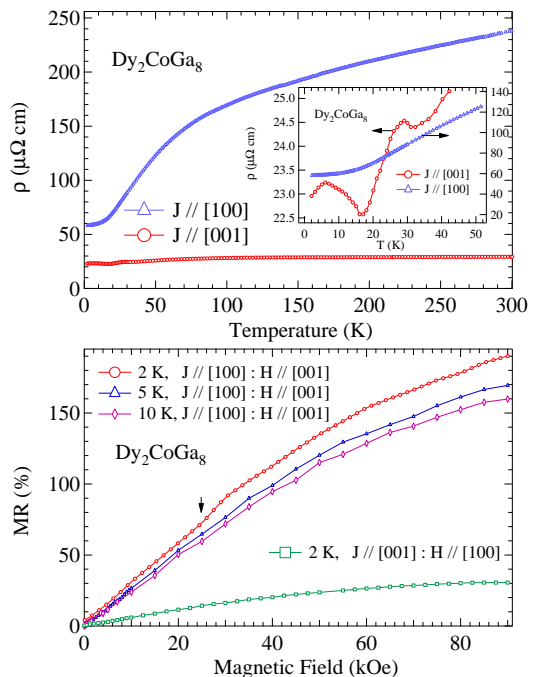


Figure 7: (a) Resistivity of Dy_2CoGa_8 with current along the two crystallographic directions, respectively; the inset shows a magnified view below 50 K; (b) Magnetoresistance at selected temperatures for configuration as mentioned in the figure.

for Y_2CoGa_8 . However, this needs further investigation. The magnetoresistance at 2 K with $J // [001]$ and $H // [100]$ as depicted in Fig. 7(b) is similar to Tb_2CoGa_8 and it increases to 25 % at 90 kOe. For $J // [100]$ and $H // [001]$ there is a change in slope at 24 kOe (shown by an arrow) above which the magnetoresistance increases monotonically to 190 % at 90 kOe. With increase in the temperature the magnetoresistance decreases and shows a negative curvature indicating the onset of field induced ferromagnetic behavior. The heat capacity of Dy_2CoGa_8 is shown in Fig 8(a). A lambda type anomaly indicates the magnetic transition. Application of a magnetic field of 50 kOe results in two humps. The effect is similar to that observed in Tb_2CoGa_8 . The $4f$ contribution to the heat capacity of Dy_2CoGa_8 and the Schottky curve calculated as explained above are shown in Fig. 8(b). In the paramagnetic regime, C_{Sch} and C_{4f} are in fair qualitative agreement with each other. S_{4f} and S_{Sch} are seen to approach the theoretically expected value at high temperatures. It may be mentioned here that Dy is a Kramer's ion, and the CEF levels in the tetragonal point symmetry will split into 8 doublets (author?) [1]. But the calculated C_{Sch} and S_{Sch} do not take into account the contribution ($R \ln 2$) from the doublet ground state. Therefore, we have shifted up our plot of S_{Sch} up by $R \ln 2$.

Ho_2CoGa_8 orders antiferromagnetically at 6 K with easy axis of magnetization along the [001] direc-

tion(author?) [1]. The resistivity of the compound is shown in Fig. 9(a) with the magnified low temperature part as an inset. The resistivity shows a drop at the ordering temperature of the compound with current parallel to [100] and [001] directions. The overall electrical resistivity with $J // [100]$ is similar to that observed by Adriano et al.(author?) [17]. Similar to the other members of the series, the resistivity with current parallel to [100] is higher than with the current parallel to [001]. Below 100 K CEF effects manifest in a relatively faster decrease of the resistivity with temperature along both the directions. The magnetoresistance of the compound is shown in Fig. 9(b) with the indicated direction of current and field. The magnetoresistance with $J // [100]$ and $H // [001]$ increases with field up to $\approx 102\%$ at 90 kOe while the corresponding variation with $J // [001]$ and $H // [100]$ is $\approx 40\%$. The high magnetoresistance with $H // [001]$ is in agreement with the easy axis of magnetization [001] of the compound. The heat capacity of Ho_2CoGa_8 plotted in Fig. 10(a) shows a sharp lambda type anomaly at the magnetic ordering temperature of the compound. The peak shifts to lower temperatures in an applied field of 30 kOe as anticipated for an antiferromagnetically ordered compound. On further increasing the field to 100 kOe the peak disappears completely and the heat capacity shows a large hump centered at 8 K. Both these effects most likely arise from the metamag-

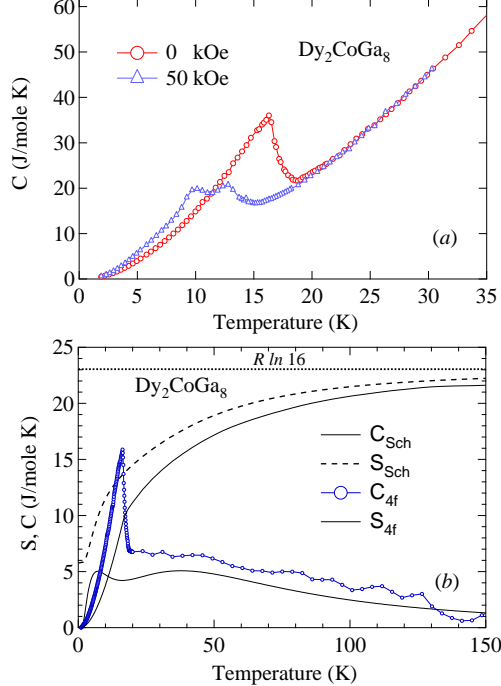


Figure 8: (a) Heat capacity of Dy_2CoGa_8 . (b) The 4f contribution to the heat capacity of Tb_2CoGa_8 with Schottky fit estimated from CEF split energy levels. The entropy estimated from magnetic contribution and CEF split levels are also shown.

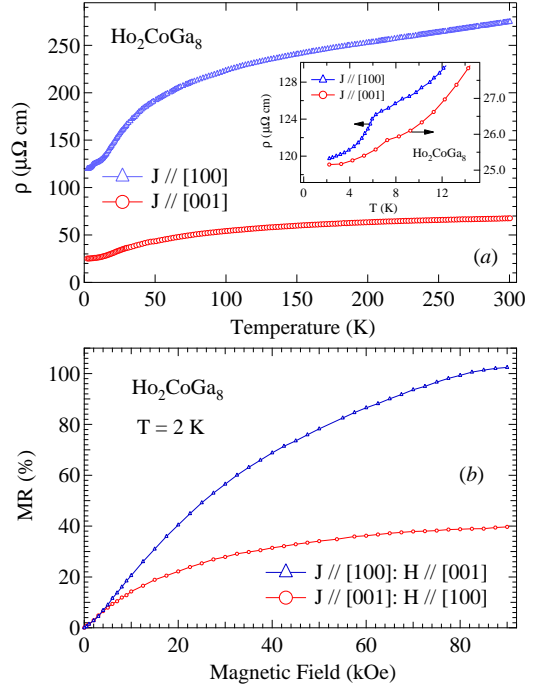


Figure 9: (a) Resistivity of Ho_2CoGa_8 with current parallel to [100] and [001], respectively with inset showing the magnified low temperature part. (b) Magnetoresistance at 2 K with current and field parallel to the indicated directions.

netic transition in the compound. The 4f contribution to the heat capacity of Ho_2CoGa_8 and the Schottky curve is shown in Fig. 10(b). The Schottky curve shows a peak and hump in fair agreement with the experimental curve. The estimated entropies from the 4f contribution to the heat capacity and the Schottky energy levels are almost equal to the theoretically expected value of $R \ln 17$.

D. Er_2CoGa_8 and Tm_2CoGa_8

In case of Er_2CoGa_8 and Tm_2CoGa_8 the easy axis of magnetization is along the ab -plane, unlike the other compounds described above where the easy axis of magnetization was along the [001] direction. These two compounds order antiferromagnetically at 3 K and 2 K, respectively(author?) [1]. The resistivity of both the compounds is shown in Fig. 11. For Er_2CoGa_8 (Fig. 11(a)) the resistivity decreases linearly from room temperature as expected for a metallic compound down to 100 K. Below 100 K the faster drop is attributed to crystal field effects. The inset shows the low temperature part of the resistivity. When $J // [100]$ the resistivity increases below ≈ 6 K followed by the downward drop for $T < T_N$ and with $J // [001]$ the resistivity falls below ≈ 6 K. The upturn in the resistivity with $J // [100]$ below 6 K can occur due to the presence of short range antiferromagnetic correlations along the ab plane which incidentally is

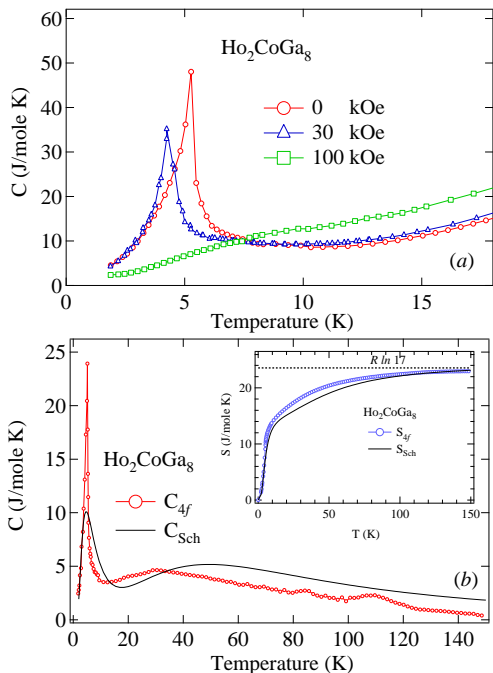


Figure 10: (a) Heat Capacity of Ho_2CoGa_8 in applied fields of 0, 30 and 100 kOe. (a) The $4f$ contribution to the heat capacity of Ho_2CoGa_8 and the Schottky heat capacity curve estimated from CEF split energy levels. The entropies estimated from the $4f$ contribution and CEF split levels are shown in the inset.

the easy axis of magnetization. The drop in the resistivity at T_N (3 K) is due to disappearance of spin disorder resistivity. The electrical resistivity for $J // [001]$ direction shows a drop exactly at the same temperature (6 K) where there was an increase in the resistivity along the other direction. Although the exact reason for this behavior is not known at present, we tentatively attribute it to the short range correlations of the moments along the easy axis. These relatively opposite variations in the thermal variation of the resistivity indicate that the configurations of the moments when resolved along different directions can be different. Compared to relatively simple ferromagnets, magnetic moments in antiferromagnetic compounds can have very complicated alignments described by a number of wave vectors, phase angles, etc. In case of Tm_2CoGa_8 the high temperature resistivity has the behavior similar to that of Er_2CoGa_8 and at low temperatures the resistivity falls at the Neel temperature (2 K) of the compound. The magnetoresistance at 2 K for Er_2CoGa_8 and Tm_2CoGa_8 is shown in Fig. 12.

The magnetoresistance for Er_2CoGa_8 with $H // [100]$ and $[001]$ respectively are close to each other up to 30 kOe. At higher fields the magnetoresistance with $H // [100]$ is marginally higher and attains a maximum value of $\approx 23\%$ at 90 kOe. The result is consistent with lesser anisotropic magnetic behavior seen in the magnetization data; also the MR is measured close to the ordering tem-

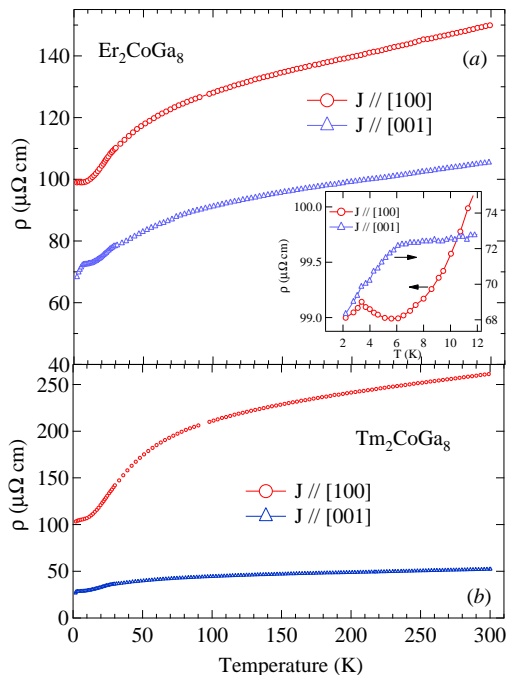


Figure 11: (a) Resistivity of Er_2CoGa_8 with current parallel to $[100]$ and $[001]$ directions respectively; the inset shows the low temperature part, (b) Resistivity of Tm_2CoGa_8 with current parallel to $[100]$ and $[001]$ directions.

perature of the compound. In case of Tm_2CoGa_8 the magnetoresistance with $J // [001]$ and $H // [100]$ is higher than that with $J // [100]$ and $H // [001]$ below 30 kOe but at higher fields the latter dominates up to the highest applied field. The magnetoresistivity at 90 kOe with $H // [001]$ is 70 % and 50 % for $H // [100]$. The initial high value of magnetoresistance for $J // [001]$ and $H // [100]$ can be understood by the fact that $[100]$ is the easy axis of magnetization for the compound. Above ≈ 30 kOe the magnetoresistance tends to saturate with field along $[100]$ direction indicating the development of the ferromagnetic component (-ve component). With field along the hard direction $[001]$ the development of ferromagnetic component will be achieved at higher fields and because of this the magnetoresistance increases leading to the observed crossover. The heat capacity of both the compounds is shown in Fig. 13. Er_2CoGa_8 shows an anomaly at the ordering temperature (3 K) while the up turn below 3 K is precursor to the magnetic transition at 2 K in Tm_2CoGa_8 . Since the heat capacity is still large at the lowest temperature data point in Er_2CoGa_8 and it is necessary to have the heat capacity data to lower temperatures in both the Er and Tm compounds, it is not possible to calculate S_{4f} in these two compounds. The $4f$ contribution to the heat capacity of Tm_2CoGa_8 and the Schottky curve is shown in Fig. 14. The Schottky curve shows a low temperature rise and hump in fair agreement with the experimental curve. A similar analysis for

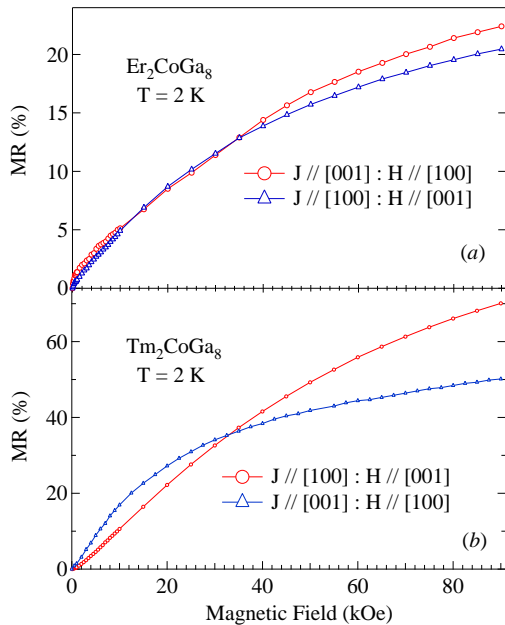


Figure 12: Magnetoresistance of Er_2CoGa_8 and Tm_2CoGa_8 at 2 K with current and field parallel to the indicated directions.

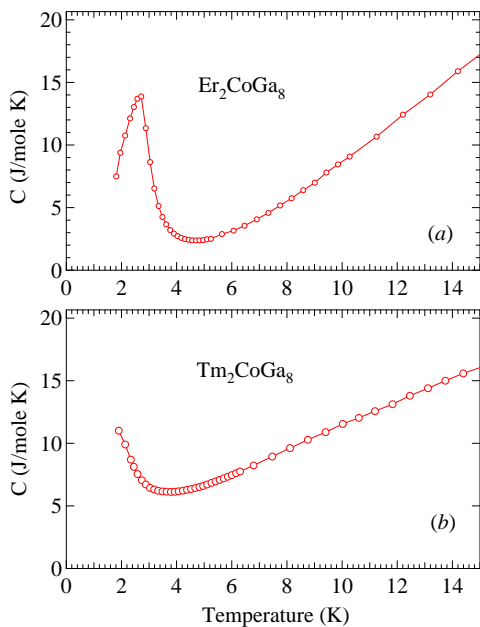


Figure 13: Heat capacity of Er_2CoGa_8 and Tm_2CoGa_8

Er_2CoGa_8 is not shown because the C_{Sch} calculated from the CEF energy levels as deduced from the magnetization data [1] did not match well with $4f$ contribution to the heat capacity.

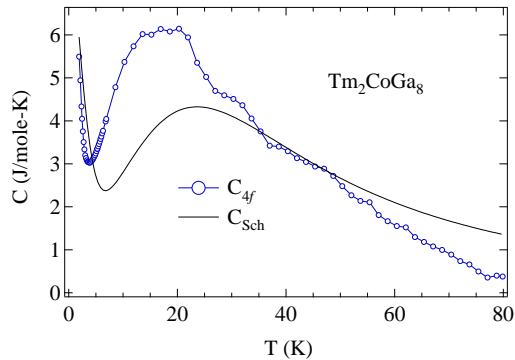


Figure 14: The $4f$ contribution to the heat capacity and the Schottky heat capacity of Tm_2CoGa_8 .

E. Conclusion

To conclude, we have studied the anisotropic electrical resistivity, magnetoresistance and heat capacity of R_2CoGa_8 single crystals. Heat capacity data provide evidence of bulk magnetic transitions with ordering temperatures matching with our earlier magnetization studies. The effect of external magnetic field on the heat capacity of these compounds is in conformity with their antiferromagnetic nature. The Schottky heat capacity calculated from the CEF energy levels derived from the magnetization data compares well with $4f$ contribution to the heat capacity in the paramagnetic regime for $\text{R} = \text{Tb}, \text{Dy}, \text{Ho}$ and to a lesser extent in Tm_2CoGa_8 , thus strengthening the validity of the CEF level scheme obtained in ref. [1] for these compounds. The electrical resistivity shows a significant anisotropy, the resistivity along the ab plane being higher compared to its magnitude along the c -axis. This anisotropic transport behavior indicates a dominant electron motion along the c -axis and may arise due to the structural anisotropy of the compound. Anomalous upturn in the electrical resistivity of some compounds as T_N is approached from the paramagnetic side is attributed to short range antiferromagnetic correlations. A hump in the non-magnetic Y_2CoGa_8 and Dy_2CoGa_8 near 29 K is tentatively attributed to CDW ordering, which needs to be probed further for confirmation. The highly anisotropic magnetoresistance data reflect the effect of metamagnetic transition in these compounds.

[1] Devang A. Joshi, R. Nagalakshmi, S.K. Dhar and A. Thamizhavel, Phys. Rev. B **77**, 174420 (2008).
 [2] Devang A. Joshi, C.V. Tomy and S.K. Malik, J. Phys.:

Condens. Matter, **19**, 136216 (2007).
 [3] C. Koenig, Z. Phys. B **50**, 33 (1983).
 [4] F. Soto, H. Berger, L. Cabo, C. Carballeira, J. Mosqueira,

- D. Pavuna, and F. Vidal, *Phys. Rev. B* **75**, 094509 (2007).
- [5] R. A. Craven and S. F. Meyer, *Phys. Rev. B* **16**, 4583 (1977).
- [6] J. A. Hofmann, A. Paskin, K.J. Tauer and R.J. Weiss, *J. Phys. Chem. Solids*, **1**, 45 (1956).
- [7] Tomoyuki Sekine, Yoshinari Kiuchi, Etsuyuki Matsuura, Kunimitsu Uchinokura and Ryozo Yoshizaki, *Phys. Rev. B* **36**, 3153 (2007).
- [8] C. Felser, E. W. Finckh, H. Kleinke, F. Rocker and W. Tremel, *J. Mater. Chem.*, **8**, 1787 (1998).
- [9] K. D. Myers, S. L. Bud'ko, I. R. Fisher, Z. Islam, H. Kleinke, A. H. Lacerda and P. C. Canfield, **205**, 27 (1999).
- [10] M. B. Fontes, J. C. Trochez, B. Giordanengo, S. L. Bud'ko, D. R. Sanchez, E. M. Baggio-Saitovitch and M. A. Continentino, *Phys. Rev. B* **60**, 6781 (1999).
- [11] R. J. Elliott and F. A. Wedgwood, *Proc. Phys. Soc.*, **81**, 846 (1963).
- [12] Y. Suezaki and H. Mori, *Prog. Theor. Phys.* **41**, 1177 (1969) and *Phys. Lett.* **28A**, 70 (1969).
- [13] I. Balberg, *Physica* **91B**, **71** (1977).
- [14] G. T. Meaden, N. H. Gsze and J. R. Jonstoan (1972), *Dynamical Aspect of critical Phenomina*, Ed. J. I. Budnik and M. P. Kawatra (New York; Gordon and Bridge), page 315.
- [15] Surjeet Singh and S. K. Dhar, *J. Phys.: Condens. Matter*, **14**, 11795 (2002).
- [16] V. Sechovsky, F. Honda, B. Janousova, K. Prokes, P. Svoboda, O. Syshchenko, A.V. Andreev, *Physica B* **328**, 95 (2003).
- [17] C. Adriano, L. Mendonça-Ferreira, E. M. Bittar and P. G. Pagliuso, *J. Appl. Phys.*, **103**, 07B712 (2008).